Pergamon

Int. J. Heat Mass Transfer. Vol. 37, No. 3, pp. 451–460, 1994

0017-9310/94 $6.00+0.00

Variational calculation of the effective emissivity for a random bed

YONG XIA and WILLIAM STRIEDER†

Department of Chemical Engineering, University of Notre Dame, Notre Dame, IN 46556, U.S.A.

(*Received* 5 *February* 1993 *and in final form* 22 *July* 1993)

Abstract—Rigorous variational upper bounds are formulated for the effective emissivity of an isothermal semi-infinite slab with an arbitrary void–solid distribution. Explicit calculations are given for a model pore structure, a semi-infinite slab cut from a bed of randomly placed freely overlapping solid spheres all of the same radius. The variational effective emissivity increases linearly with the void fraction, and the slope of this increase depends on the particle surface emissivity. The variational upper bound and a recently obtained lower, truncated multiple scattering summation bound provide a rigorous squeeze on the effective emissivity curves, which tightens with decreasing void fraction. These reciprocal bounds are compared with cell model and two-flux bed emissivities as well as available experimental data.

INTRODUCTION

To develop the solution of the engineering heat transfer equations, including high temperature radiation from the external boundary of a randomly dispersed solid bed to the surroundings, requires a knowledge of the effective bed emissivity ε_{eff}. Radiative losses from the external boundaries of porous solid reactant compacts [1] play an important role in the high temperature combustion synthesis of advanced ceramic materials. The external circumference of the pressed cylindrical pellets used to make silicon nitride may reach 4000°C as the reaction wave passes. On the other hand, to sustain non-catalytic, materials processing, gas–solid reactions, such as the reduction of ores or the roasting of sulfides, depends on a net transfer of radiant heat to the porous outer shell [2] of the reacting particle. The fluidized bed regeneration [3] of cracking catalyst porous pellets is another case of a high temperature chemical industrial process, where effective radiant transfer coefficients would be useful for the selection of optimum thermal conditions. Effective bed emissivity values are also needed for the design of fluidized bed solar collectors [4].

In previous theoretical work by others, Brewster [5, 6], using the two-flux model, derived an expression for the effective bed emissivity of an isothermal bed of dispersed solid particles. Tien and Drolen [7] have pointed out that the two-flux model can be inaccurate in an anisotropically scattering dispersion such as a fluidized bed. Also the bed scattering coefficients used by Brewster [6] limit any application to dilute particle beds.

Borodulya *et al.* [8, 9] in their calculation of ε_{eff} for an isothermal bed model the bed structure as a stationary cubic lattice of solid spherical particles. In order to treat a single unit cell of the lattice as a closed system, the cell faces that cut the void space are assumed to be black, diffusive planar surfaces. In addition approximate network theory [10] was used. Vortmeyer [11], in his review of radiation transport models in packed solids, has observed that, as a result of these approximations, cell models do not include long range scattering in a rigorous manner. Borodulya *et al.* [8] generated numerical values of ε_{eff} only for two specific porosities, a packed ($\phi = 0.4$) and expanded lattice ($\phi \geqslant 0.95$).

Measurements of high temperature fluidized bed to wall radiation is difficult and expensive [12]. Grace [13] in *Handbook of Multiphase Systems* does list four experimentally measured effective bed emissivities along with the corresponding particle emissivities, but no information about the spatial particle arrangement or bed porosity is given. Grace [13] has also proposed an empirical relationship between the effective emissivity of a fluidized bed and the particle emissivity, which does not contain the porosity. In general, these efforts have not produced a clear, systematic dependence of ε_{eff} on bed structure.

Variational principles have been used in heterogeneous, multiphase engineering media to successfully estimate other effective transport coefficients and thermodynamic properties [14, 15] and we seek here to apply the method to ε_{eff}. In the next section, the fundamental equations for the transport, reflection and absorption will be formulated. In the third section, we will derive a new, rigorous variational upper bound on the effective bed emissivity, whose true value is equivalent to the exact solution of the random bed radiative heat, effective emissivity problem. The variational bounds are expressed in terms of certain averages that characterize the essen-

† Author to whom correspondence should be addressed.

NOMENCLATURE

$B(\mathbf{r})$ radiosity

$f(x, \rho, \eta, \eta')\, d^3\rho\, d^2\eta\, d^2\eta'$ the probability that two points $\mathbf{r}$ and $\mathbf{r}'$ on Σ_{int} which can see each one another, the first lying within dx, have a relative position vector ρ lying in $d^3\rho$, and that η falls within $d^2\eta$ and η' in $d^2\eta'$

$h(x, \rho, \eta)\, d^2\rho\, d^2\eta$ the probability that two points that can see one another, the first point taken on Σ_{int} within dx and second on Σ_o, have a relative position vector ρ lying within $d^2\rho$, and a unit normal η at the first point is within $d^2\eta$

$K(\mathbf{r}', \mathbf{r})\, d^2\mathbf{r}$ differential view factor from $\mathbf{r}'$ to $d^2\mathbf{r}$ located at $\mathbf{r}$

m $4\phi/s$, $4\times$ void fraction/surface area per unit total volume

$P(\mathbf{r})$, $P^*(\mathbf{r})$ surface radiosity minus the black surface radiosity, and trial function

$u(\eta)\, d^2\eta$ the probability that a point on Σ_{int} has η falling within $d^2\eta$

x perpendicular distance from the $x = 0$ plane to a point in the bed.

Greek symbols

$\Gamma\{P^*\}$ variational functional

δP the first order variation of P^* function

ε emissivity

η surface unit normal

λ radiation penetration parameter given in trial function (27) and Fig. 2(a)

ρ displacement vector, $\mathbf{r}' - \mathbf{r}$

$\sigma_i(x)$ the mean surface area that can be seen from a typical internal point within dx

$\sigma_o(x)$ the mean area on Σ_o that can be seen from an internal surface point within dx

Σ surface area.

Subscripts

ext solid surface at the edge of the bed

int internal solid surface

o wall of the bed

s void–solid interface.

tial features of any arbitrary, random geometry in the fourth section. To illustrate the method in a manageable, yet useful model random bed, a variational effective emissivity equation, for a semi-infinite slab cut from a bed of randomly placed, freely overlapping solid spheres all of the same radius, is presented. From an entirely different path summation approach, complementary upper and lower bounds [16] have been obtained for the same model system. The variational principle does give significantly improved upper bounds, and along with the lower sum bound provides a squeeze useful for the prediction of ε_{eff}. The effective emissivity values compare quantitatively with the two-flux and cell model, lattice results. The experimental data lie within the predictive bounds.

BASIC EQUATIONS

For high temperature transport processes within porous solids, there are a number of instances [1, 2, 17] where the temperature gradients normal to the porous solid external surface can be neglected, and the surface radiation term is either locally isothermal in the differential element, or is globally isothermal. In the second case of a high temperature fluidized bed, due to the high degree of solid particle mixing, an isothermal bed is often a reasonable first approximation. Indeed, for large particle fluidized beds (diameter >1 mm), isothermal conditions are an accurate assumption [13, 18, 19]. In this paper expressions for the effective emissivity are developed for a void–solid system of arbitrary geometry and a uniform temperature T_s.

We will consider the characteristic diameter of the solid particles used to construct the void–solid distribution as sufficiently larger than the wavelength of the thermal radiation [10], and the characteristic distance between neighboring solid particles as small enough [8, 9], that the radiative transfer may be regarded as occurring due to multiple optical reflections at the void–solid interface. For the formulation of the equations, a semi-infinite slab (Fig. 1) of dis-

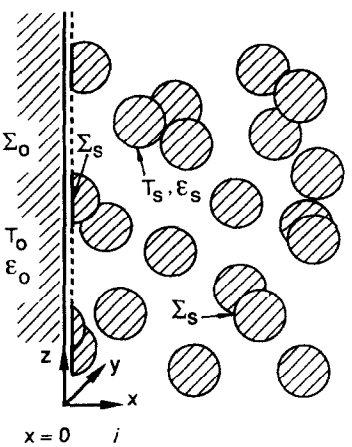

FIG. 1. Semi-infinite slab of randomly overlapping solid spheres.

tributed solid runs in the direction of a unit vector **i** from $x = 0$ in the positive direction to infinity. The solid is opaque with gray emitting–diffusely reflecting surfaces. Kirchhoff's law is assumed [10]. The void gas is taken to be transparent. Though a specific structure is shown in Fig. 1, for the formulation of the equations and the variational principle the void–solid geometry is arbitrary. The void–solid interface Σ_s is made up of internal surfaces and may in some cases include an edge surface at $x = 0$. The surface Σ_s has a constant temperature T_s and local emissivity ε_s. Just outside the end of the semi-infinite slab, an infinite plane wall Σ_o, at temperature T_o and emissivity ε_o is located.

The effective bed emissivity ε_{eff} is the net result of the infinitely many possible exit paths that radiation emitted from the void–solid interface (or particle surface) may take. Each of these paths starts with emission from Σ_s, the radiation then travels across the void space either directly in a single straight line path or in some unbroken sequence of straight line segments alternating with diffuse surface reflections, and the path ends when the radiation passes out to the slab edge plane Σ_o. In the case of the external edge of a porous particle, the edge surface Σ_o represented in Fig. 1 may not be present as a solid wall. Then Σ_o plays the role of a mathematical surface, across which the emitted photon must pass to escape and T_o is set to zero in the basic equations. For a gray diffuse surface Σ_s, the effective bed emissivity depends solely on the bed particle surface emissivity ε_s, that governs the surface interactions, and the statistical properties of the bed structure, which determine the geometry of the radiation paths. Since our goal is an a priori value of the bed emissivity ε_{eff} and since it does not depend on the external wall emissivity, we consider the special case of Σ_o as a black wall with emissivity $\varepsilon_o = 1$, set the net flux Q of heat into the bed

$$Q = \varepsilon_{eff}\sigma(T_o^4 - T_s^4), \tag{1}$$

and claim no loss in generality in the values of ε_{eff}. Note that (1) is obtained directly from the definition of ε_{eff} along with Kirchhoff's law [10], and that σ is the Stefan–Boltzmann constant.

The radiation is emitted and reflected diffusely according to Lambert's cosine law [10]. The emitted flux depends on the absolute temperature T of the surfaces Σ_o or Σ_s, the surface emissivity ε, and the Stefan–Boltzmann constant σ in the combination $\varepsilon\sigma T^4$. Kirchhoff's law states that the same surface element will absorb only the fraction ε of incident radiation, reflecting the fraction $(1-\varepsilon)$. If H represents the radiant flux incident on a unit surface of Σ_o or Σ_s, then for a diffusely reflecting surface the radiosity B, the radiation diffusely leaving a unit surface, is given by

$$B(\mathbf{r}) = \varepsilon\sigma T^4 + (1-\varepsilon)H \quad (\mathbf{r} \text{ on } \Sigma_o \text{ or } \Sigma_s). \tag{2}$$

If the surface point **r** is located on Σ_o or Σ_s and **r**′ is also on Σ_o or Σ_s, the fraction $K(\mathbf{r}', \mathbf{r})\,\mathrm{d}^2\mathbf{r}$ of radiation diffusely distributed, from a unit surface element located at **r**′, that travels a straight line free path, and arrives at a second surface element $\mathrm{d}^2\mathbf{r}$ located at **r**, can be used to formulate the radiant exchange between these surfaces. Since we are assuming diffuse scattering at the wall surfaces, K is given by cosine law

$$K(\mathbf{r}, \mathbf{r}') = \begin{cases} -[\boldsymbol{\eta}(\mathbf{r})\cdot\boldsymbol{\rho}][\boldsymbol{\eta}(\mathbf{r}')\cdot\boldsymbol{\rho}]/(\pi\rho^4) & (\text{if } \mathbf{r} \text{ can see } \mathbf{r}') \quad (3) \\ 0 & (\text{otherwise}) \quad (4) \end{cases}$$

where $\boldsymbol{\eta}(\mathbf{r})$ and $\boldsymbol{\eta}(\mathbf{r}')$ are unit normals, respectively, at any points **r** and **r**′ on the surface of Σ_o or Σ_s pointing into the void, and $\boldsymbol{\rho} = (\mathbf{r}' - \mathbf{r})$. The symmetry property

$$K(\mathbf{r}, \mathbf{r}') = K(\mathbf{r}', \mathbf{r}) \tag{5}$$

holds for all **r** and **r**′ in any pair combination of Σ_o or Σ_s.

Of the diffuse radiation $B(\mathbf{r}')\,\mathrm{d}^2\mathbf{r}'$ leaving $\mathrm{d}^2\mathbf{r}'$ of Σ_o or Σ_s, only the fraction $B(\mathbf{r}')\,\mathrm{d}^2\mathbf{r}'K(\mathbf{r}', \mathbf{r})\,\mathrm{d}^2\mathbf{r}$ will arrive within the element of surface area $\mathrm{d}^2\mathbf{r}$ at **r**, then the total incident flux $H(\mathbf{r})$ to a unit area of surface at **r** is

$$\int_{\Sigma_o+\Sigma_s} \mathrm{d}^2\mathbf{r}'K(\mathbf{r}', \mathbf{r})B(\mathbf{r}') = H(\mathbf{r}) \quad (\mathbf{r} \text{ on } \Sigma_s \text{ or } \Sigma_o). \tag{6}$$

From the radiosity definition (2) and equation (6), an integral equation for the radiosity is obtained

$$B(\mathbf{r}) = \varepsilon_s\sigma T_s^4 + (1-\varepsilon_s)\int_{\Sigma_o+\Sigma_s} \mathrm{d}^2\mathbf{r}'K(\mathbf{r}', \mathbf{r})B(\mathbf{r}') \quad (\mathbf{r} \text{ on } \Sigma_s). \tag{7}$$

Equation (7) together with the steady state boundary condition

$$B(\mathbf{r}) = \sigma T_o^4 \quad (\mathbf{r} \text{ on } \Sigma_o) \tag{8}$$

are in principle sufficient to determine B. In practice the complex geometry of the surface Σ_s prevents an outright solution. Suppose we are positioned deep within the bed at **r** on Σ_s. Any radiation from Σ_o at T_o is absorbed before it reaches **r**, and from **r** the bed conditions appear to be uniform. The surface point at **r** does not receive radiation from Σ_o or from Σ_s surfaces located near $x = 0$, **r** only receives radiation from bed surfaces at a constant T_s and ε_s, $B(\mathbf{r})$ is locally constant, and the radiosity comes out of the integral in (7). The remaining integral of $K(\mathbf{r}', \mathbf{r})$ over Σ_o and Σ_s is unity, and we have

$$B(\mathbf{r}) = \sigma T_s^4 \quad (\mathbf{r} \text{ on } \Sigma_s \text{ deep within bed}). \tag{9}$$

We can define a new variable to describe the radiosity increase ($T_o > T_s$) or decrease ($T_o < T_s$) due to hot or cold photon radiation from the wall Σ_o

$$P(\mathbf{r}) = B(\mathbf{r}) - \sigma T_s^4 \tag{10}$$

and reformulate (7) and (8) into

$$P(\mathbf{r}) = (1-\varepsilon_s)\int_{\Sigma_o+\Sigma_s} d^2\mathbf{r}' K(\mathbf{r}',\mathbf{r})P(\mathbf{r}')$$

$$(\mathbf{r} \text{ on } \Sigma_s) \qquad (11)$$

with

$$P(\mathbf{r}) = \sigma T_o^4 - \sigma T_s^4 \quad (\mathbf{r} \text{ on } \Sigma_o). \qquad (12)$$

Finally the net flux Q from the wall into the bed is simply the radiation emitted by the wall Σ_o, minus the radiation emitted or reflected from the bed surfaces Σ_s that travel out of the bed to strike Σ_o

$$Q = \sigma T_o^4 - \Sigma_o^{-1}\int_{\Sigma_o} d^2\mathbf{r}\int_{\Sigma_s} d^2\mathbf{r}' K(\mathbf{r},\mathbf{r}')B(\mathbf{r}'). \qquad (13)$$

Note that a knowledge of $B(\mathbf{r})$ from (11) and (12), allows first the calculation of Q from (13), then through (1) the calculation of ε_{eff}, and the symmetry property (5) has been employed.

VARIATIONAL FORMULATION

In this section we will derive a variational upper bound on the wall to random bed heat flux and then on the effective bed emissivity. The upper bound is based on the variational functional

$$\Sigma_o\Gamma\{P^*\} = -2\int_{\Sigma_s} d^2\mathbf{r}\int_{\Sigma_o} d^2\mathbf{r}'(1-\varepsilon_s)K(\mathbf{r}',\mathbf{r})P^*(\mathbf{r})P(\mathbf{r}')$$

$$-\int_{\Sigma_s} d^2\mathbf{r}\int_{\Sigma_s} d^2\mathbf{r}'(1-\varepsilon_s)K(\mathbf{r}',\mathbf{r})P^*(\mathbf{r})P^*(\mathbf{r}')$$

$$+\int_{\Sigma_s} d^2\mathbf{r}[P^*(\mathbf{r})]^2 \qquad (14)$$

where the trial function $P^*(\mathbf{r})$ must satisfy

$$P^*(\mathbf{r}) = P(\mathbf{r}) = \sigma T_o^4 - \sigma T_s^4 \quad (\mathbf{r} \text{ on } \Sigma_o). \qquad (15)$$

To show that the term $\delta\Gamma$ from (14), first order in the variation δP of the trial function P^* about P vanishes, we write

$$\tfrac{1}{2}\Sigma_o\delta\Gamma = -\int_{\Sigma_s} d^2\mathbf{r}\int_{\Sigma_o} d^2\mathbf{r}'(1-\varepsilon_s)K(\mathbf{r}',\mathbf{r})\delta P(\mathbf{r})P(\mathbf{r}')$$

$$-\int_{\Sigma_s} d^2\mathbf{r}\int_{\Sigma_s} d^2\mathbf{r}'(1-\varepsilon_s)K(\mathbf{r}',\mathbf{r})\delta P(\mathbf{r})P(\mathbf{r}')$$

$$+\int_{\Sigma_s} d^2\mathbf{r}\delta P(\mathbf{r})P(\mathbf{r}). \qquad (16)$$

The symmetry property (5) of K, with the interchange of the integration variables $\mathbf{r}$ and $\mathbf{r}'$, was used to obtain the middle term in the right-hand side of (16). A necessary and sufficient condition that the first order term $\delta\Gamma$ in the variation of (14) vanish is that P in equation (16) is the solution of (11). Note also that $P(\mathbf{r})$ without the asterisk, does not vary from condition (15), i.e.

$$\delta P(\mathbf{r}) = 0 \quad (\mathbf{r} \text{ on } \Sigma_o). \qquad (17)$$

To fix a sign on the second order term $\delta^2\Gamma$ in the variation of (14), we recast (14) in a somewhat different form

$$\Gamma\{P^*\} = -2\Psi + \Lambda \qquad (18)$$

where

$$\Sigma_o\Psi = \int_{\Sigma_s} d^2\mathbf{r}\int_{\Sigma_o} d^2\mathbf{r}'(1-\varepsilon_s)K(\mathbf{r}',\mathbf{r})P^*(\mathbf{r})P(\mathbf{r}') \qquad (19)$$

and

$$\Sigma_o\Lambda = \frac{1}{2}\int_{\Sigma_s} d^2\mathbf{r}\int_{\Sigma_s} d^2\mathbf{r}'(1-\varepsilon_s)K(\mathbf{r}',\mathbf{r})[P^*(\mathbf{r})-P^*(\mathbf{r}')]^2$$

$$+\int_{\Sigma_s} d^2\mathbf{r}[P^*(\mathbf{r})]^2\left[1-\int_{\Sigma_s} d^2\mathbf{r}'(1-\varepsilon_s)K(\mathbf{r}',\mathbf{r})\right]. \qquad (20)$$

Once again the symmetry condition (5) on K upon interchange of $\mathbf{r}$ and $\mathbf{r}'$, allow us to relate the $[P^*(\mathbf{r})]^2K$ and $[P^*(\mathbf{r}')]^2K$ type terms in (20) so that they cancel out to retrieve (14). Note that Ψ does not produce a second order term in δP. The sense of the inequality derives from Λ and the interpretation of $K\,d^2\mathbf{r}$ as a positive fraction, whose total summing $d^2\mathbf{r}$ over all $\Sigma_o+\Sigma_s$ is unity. Since both K and

$$\left[1-(1-\varepsilon_s)\int_{\Sigma_s} K(\mathbf{r}',\mathbf{r})\,d^2\mathbf{r}'\right]$$

are positive, the second order terms in Λ and Γ are positive and

$$\Gamma\{P\} \leqslant \Gamma\{P^*\}. \qquad (21)$$

To interpret $\Gamma\{P\}$, we return to equation (14) and substitute equation (11) directly into $\Gamma\{P\}$ and obtain

$$\Sigma_o\Gamma\{P\} = -(1-\varepsilon_s)\int_{\Sigma_s} d^2\mathbf{r}\int_{\Sigma_o} d^2\mathbf{r}'K(\mathbf{r}',\mathbf{r})P(\mathbf{r})P(\mathbf{r}'). \qquad (22)$$

Direct substitution of (10) and (12) into equation (22) gives us

$$\Sigma_o\Gamma\{P\} = (\sigma T_o^4 - \sigma T_s^4)\sigma T_s^4(1-\varepsilon_s)$$

$$\times\int_{\Sigma_s} d^2\mathbf{r}\int_{\Sigma_o} d^2\mathbf{r}'K(\mathbf{r}',\mathbf{r}) - (\sigma T_o^4 - \sigma T_s^4)(1-\varepsilon_s)$$

$$\times\int_{\Sigma_s} d^2\mathbf{r}\int_{\Sigma_o} d^2\mathbf{r}'K(\mathbf{r}',\mathbf{r})B(\mathbf{r}). \qquad (23)$$

Then the first integral in (23) is equal to the surface area Σ_o of the external wall, the second integral upon interchange of $\mathbf{r}$ and $\mathbf{r}'$ is related to Q by (13)

$$\Gamma\{P\} = -(\sigma T_o^4 - \sigma T_s^4)^2(1-\varepsilon_s)$$

$$+(\sigma T_o^4 - \sigma T_s^4)(1-\varepsilon_s)Q, \qquad (24)$$

with equation (1) for Q the zeroth order term $\Gamma\{P\}$ of the variational principle can be written directly in terms of the effective bed emissivity, and the sub-

stitution of the variational inequality (21) gives the variational principle for the effective bed emissivity

$$\varepsilon_{\text{eff}} \leqslant 1+\Gamma\{P^*\}(1-\varepsilon_s)^{-1}(\sigma T_o^4-\sigma T_s^4)^{-2}. \quad (25)$$

When the trial function P^* is replaced in (25) and (14) by the true solution P of (11) and (12), the equality is obtained. A complete solution P of the wall to bed radiation heat transport problem is required for a full knowledge of ε_{eff}, any other trial P^* gives a rigorous upper bound. The variational inequality (25) can be rewritten in terms of the functional Ψ and Λ equations, (19) and (20), respectively

$$\varepsilon_{\text{eff}} \leqslant 1+(\Lambda-2\Psi)(1-\varepsilon_s)^{-1}(\sigma T_o^4-\sigma T_s^4)^{-2}. \quad (26)$$

To proceed further with the evaluation of Ψ and Λ from (19) and (20), we note that in some instances, e.g. a slab cut from a porous material or a pressed compact, the surface of the random solid may be divided into two parts (Fig. 1), an external part Σ_{ext} in contact with the plane $x = 0$, i.e. the plane surface of the solid cut by the $x = 0$ plane; and a finite curvature internal surface Σ_{int}, formed in Fig. 1 by the non-overlapped sphere surfaces in contact with the void volume, or more generally for any arbitrary random void–solid structure, the internal pore wall surfaces of the slab. Then if we represent the ratio of the void volume within the slab to the *internal* surface area in contact with the void as the length scale $m/4$, where m is usually called the hydraulic average pore diameter, the trial function P^* we propose for the evaluation of Ψ and Λ in terms of positive x-direction, unit vector $\mathbf{i}$ pointing into slab

$$P^*(\mathbf{r}) = [\mu+\omega\mathbf{i}\cdot\boldsymbol{\eta}(\mathbf{r})]\exp(-\lambda x/m) \quad (\mathbf{r} \text{ on } \Sigma_s), \quad (27)$$

where μ, ω and λ are variational parameters. That the trial function of the scattered radiation P^*, as defined by (9) and (10), should vanish deep within the slab is accomplished by the exponential in (27). Upon the selection of the optimum μ and ω, the trial function P^* will be positive for a hot wall temperature $T_o > T_s$ in excess of the equilibrium value T_s. For a cold wall $T_o < T_s$, or no wall at all $T_o = 0$, the radiosity at the solid edge drops below σT_s^4 and P^* is negative. $\boldsymbol{\eta}$ is again the surface unit normal at the point $\mathbf{r}$ on the void–solid interface. The $\omega\mathbf{i}\cdot\boldsymbol{\eta}$ term combined with the smooth exponential decay, fluctuates (due to the factor $\omega\mathbf{i}\cdot\boldsymbol{\eta}$) with random local structure of the void–solid interface. Note on the external surface Σ_{ext} of the random solid, the trial function has a constant value of $(\mu-\omega)$.

The variational principle (26) with the trial function (27) can be applied to many void–solid structures, e.g. fiber mats for ceramic composites, porous solids, or fixed bed packing with $\Sigma_{\text{ext}} = 0$ and $\Sigma_{\text{int}} = \Sigma_s$. Some of these applications will require computationally intense Monte Carlo calculations both to generate the beds and to evaluate the variational integrals. It is reasonable at this point to examine the characteristics and efficacy of the variational method in the context of a simpler, yet useful class of structures.

STATISTICAL CHARACTERIZATION

To obtain an idea of the statistical information needed to develop the variational forms, the bounds on the effective bed emissivity will be expressed in terms of certain averages characterizing a semi-infinite slab cut from a statistically homogeneous, isotropic random void–solid geometry. We define the void fraction ϕ as the void volume to total volume ratio, the average pore diameter m, as four times the void volume to internal surface area Σ_{int} ratio, $\sigma_i(x)$ as the average area of the internal surface Σ_{int} that can be seen from a point on the surface Σ_{int} lying within the infinitesimal slab dx and $\sigma_o(x)$ as the average area of the external wall Σ_o that can be seen from a point on the surface Σ_{int} lying within dx. In addition, we define the probability $u(\boldsymbol{\eta})\,d^2\boldsymbol{\eta}$ that an exposed surface point in the infinitesimal slab dx has a surface unit normal $\boldsymbol{\eta}$ falling within the element of solid angle $d^2\boldsymbol{\eta}$, the probability $f(x, \boldsymbol{\rho}, \boldsymbol{\eta}, \boldsymbol{\eta}')\,d^3\boldsymbol{\rho}\,d^2\boldsymbol{\eta}\,d^2\boldsymbol{\eta}'$ that two points $\mathbf{r}$ and $\mathbf{r}'$ on the internal surface Σ_{int} that can see one another, the first point taken within the infinitesimal slab dx located at x, have surface unit normals $\boldsymbol{\eta}$ and $\boldsymbol{\eta}'$ falling in the elements of solid angle $d^2\boldsymbol{\eta}$ and $d^2\boldsymbol{\eta}'$, respectively, and a relative position vector $\boldsymbol{\rho} = \mathbf{r}'-\mathbf{r}$ lying in the volume element $d^3\boldsymbol{\rho}$; and the probability $h(x, \boldsymbol{\rho}, \boldsymbol{\eta})\,d^2\boldsymbol{\rho}\,d^2\boldsymbol{\eta}$ that two points $\mathbf{r}$ and $\mathbf{r}'$ that can see one another, the first point taken from Σ_{int} within dx at x and the second on the external plane Σ_o, have a relative position vector $\boldsymbol{\rho}$ lying within the planar area element $d^2\boldsymbol{\rho}$ and a unit normal $\boldsymbol{\eta}$ at $\mathbf{r}$ within $d^2\boldsymbol{\eta}$.

The integrals (19), (20) we must evaluate to obtain the variational upper bound (26) on ε_{eff} can be expressed in terms of the probabilities defined above. From the variational principle forms (14), (18), (19) and noting that $\Sigma_s = \Sigma_{\text{ext}}+\Sigma_{\text{int}}$, we have

$$\Sigma_o\Lambda = \int_{\Sigma_{\text{ext}}+\Sigma_{\text{int}}} d^2\mathbf{r}[P^*(\mathbf{r})]^2 - \int_{\Sigma_{\text{ext}}+\Sigma_{\text{int}}} d^2\mathbf{r} \times \int_{\Sigma_{\text{ext}}+\Sigma_{\text{int}}} d^2\mathbf{r}'(1-\varepsilon_s)K(\mathbf{r}', \mathbf{r})P^*(\mathbf{r})P^*(\mathbf{r}'). \quad (28)$$

A line drawn from any point on Σ_{ext} to a point on Σ_{int} is always blocked by the solid and the corresponding $K(\mathbf{r}, \mathbf{r}')$ is zero, hence the double integrals over Σ_{ext} and Σ_{int} vanish in (28). Since $\Sigma_{\text{ext}}/\Sigma_o = 1-\phi$ and using the trial function (27),

$$\Lambda = (\mu-\omega)^2(1-\phi) + \Sigma_o^{-1}\int_{\Sigma_{\text{int}}} d^2\mathbf{r}[\mu+\omega\mathbf{i}\cdot\boldsymbol{\eta}(\mathbf{r})]^2\exp(-2\lambda x/m) - (1-\varepsilon_s)\Sigma_o^{-1}\int_{\Sigma_{\text{int}}} d^2\mathbf{r}\int_{\Sigma_{\text{int}}} d^2\mathbf{r}' \times K(\mathbf{r}', \mathbf{r})[\mu+\omega\mathbf{i}\cdot\boldsymbol{\eta}(\mathbf{r})]\cdot[\mu+\omega\mathbf{i}\cdot\boldsymbol{\eta}(\mathbf{r}')] \times \exp(-\lambda x/m-\lambda x'/m). \quad (29)$$

Then from the forms (3) and (4) of K, and the probabilities u and f defined above, we can rewrite (29) as

$$\Lambda = (\mu-\omega)^2(1-\phi)+(4\phi/m)\int \mathrm{d}x \times \int \mathrm{d}^2\boldsymbol{\eta} u(\boldsymbol{\eta})[\mu+\omega\mathbf{i}\cdot\boldsymbol{\eta}]^2 \exp(-2\lambda x/m) + (4\phi/m)\int \mathrm{d}x \int \mathrm{d}^3\boldsymbol{\rho} \int \mathrm{d}^2\boldsymbol{\eta} \int \mathrm{d}^2\boldsymbol{\eta}' \sigma_i(x) \times f(x,\boldsymbol{\rho},\boldsymbol{\eta},\boldsymbol{\eta}')[(\boldsymbol{\eta}\cdot\boldsymbol{\rho})(\boldsymbol{\eta}'\cdot\boldsymbol{\rho})/(\pi\rho^4)] \times (1-\varepsilon_s)[\mu+\omega\mathbf{i}\cdot\boldsymbol{\eta}][\mu+\omega\mathbf{i}\cdot\boldsymbol{\eta}'] \times \exp[-(\lambda x/m)-(\lambda x'/m)]. \quad (30)$$

The integrations extend over all orientations of the unit vectors $\boldsymbol{\eta}$ and $\boldsymbol{\eta}'$ subject to the conditions $\boldsymbol{\rho}\cdot\boldsymbol{\eta} \geqslant 0$ and $\boldsymbol{\rho}\cdot\boldsymbol{\eta}' \leqslant 0$, over all values of $\boldsymbol{\rho}$ for the entire semi-infinite slab, and over all values of x from zero to infinity.

The Ψ integral (19) over Σ_s can be split into separate integrals for Σ_{ext} and Σ_{int}. Upon the substitution of the $P(\mathbf{r})$ function (15) and the trial function (27), the integral (19) becomes

$$\Psi = (1-\varepsilon_s)(\sigma T_o^4-\sigma T_s^4)\left\{(\mu-\omega)\Sigma_o^{-1} \times \int_{\Sigma_{ext}} \mathrm{d}^2\mathbf{r} \int_{\Sigma_o} \mathrm{d}^2\mathbf{r}' K(\mathbf{r}',\mathbf{r}) + \Sigma_o^{-1} \int_{\Sigma_{int}} \mathrm{d}^2\mathbf{r} \times \int_{\Sigma_o} \mathrm{d}^2\mathbf{r}' K(\mathbf{r}',\mathbf{r})[\mu+\omega\mathbf{i}\cdot\boldsymbol{\eta}(\mathbf{r})]\exp(-\lambda x/m)\right\}. \quad (31)$$

The entire radiosity flux from $\mathrm{d}^2\mathbf{r}$ on the solid external surface Σ_{ext} must cross over to Σ_o, the integral of K with one point $\mathbf{r}$ located on Σ_{ext}, but evaluated over $\mathrm{d}^2\mathbf{r}'$ of Σ_o gives unity and

$$\Psi = (1-\varepsilon_s)(\sigma T_o^4-\sigma T_s^4)\left\{(\mu-\omega)(1-\phi)+\Sigma_o^{-1} \times \int_{\Sigma_{int}} \mathrm{d}^2\mathbf{r} \int_{\Sigma_o} \mathrm{d}^2\mathbf{r}' K(\mathbf{r}',\mathbf{r})[\mu+\omega\mathbf{i}\cdot\boldsymbol{\eta}(\mathbf{r})]\exp(-\lambda x/m)\right\}. \quad (32)$$

Then from the forms (3), (4) of K and the probability h

$$\Psi = (1-\varepsilon_s)(\sigma T_o^4-\sigma T_s^4)\left\{(\mu-\omega)(1-\phi) - (4\phi/m)\int \mathrm{d}x \int \mathrm{d}^2\boldsymbol{\rho} \int \mathrm{d}^2\boldsymbol{\eta}\sigma_o(x)h(x,\boldsymbol{\rho},\boldsymbol{\eta}) \times [(\boldsymbol{\eta}\cdot\boldsymbol{\rho})(\mathbf{i}\cdot\boldsymbol{\rho})/(\pi\rho^4)][\mu+\omega\mathbf{i}\cdot\boldsymbol{\eta}]\exp(-\lambda x/m)\right\}. \quad (33)$$

Again the integration is over all the orientations of the unit vector $\boldsymbol{\eta}$, subject to the condition $\boldsymbol{\rho}\cdot\boldsymbol{\eta} \geqslant 0$, over all values of $\boldsymbol{\rho}$ for the entire infinite plane surface Σ_o and over all x from 0 to ∞.

One very simple model (Fig. 1) for a random dispersion of solid is obtained when a thick slab of total volume V is cut from a very large bed of randomly placed, freely overlapping solid spheres all of the same radius q. All those points within the slab lying on the curved surface of the spheres, but not in the interior of one or more overlapping spheres, make up the interior surface Σ_{int} of the random suspension. Those surface points on the $x = 0$ edge of the slab, i.e. the flat cut surface of the sphere solid, make up the edge surface Σ_{ext} and those points on the interior of a sphere make up the solid.

The statistics of this geometry [14] is sufficiently straightforward to allow analytical forms for ϕ, s, m, σ_o, σ_i, u, h and f. For a large random bed of overlapping spheres, the probability P_v that a volume v is free of sphere centers is

$$P_v = \exp(-v\zeta) \quad (34)$$

where ζ is the density of sphere centers of the large sphere bed per unit total volume. That a point be in the void requires sphere centers be excluded from a spherical volume of radius q about the point, and the probability of finding a point in the void is just the porosity ϕ

$$\phi = \exp(-4\pi q^3\zeta/3). \quad (35)$$

The total sphere area, overlapped or not, per unit total volume is $4\pi q^2\zeta$, and the exposed (not overlapped) sphere area s per unit total volume is

$$s = 4\pi q^2\zeta\phi. \quad (36)$$

The average pore diameter m (four times void volume divided by the void surface interface area) is

$$m = 4\phi/s = (\pi q^2\zeta)^{-1}. \quad (37)$$

If we consider a point on the exposed surface of the infinitesimal slab $\mathrm{d}x$, since all values of $\boldsymbol{\eta}$ are equally likely, the probability $u(\boldsymbol{\eta})\,\mathrm{d}^2\boldsymbol{\eta}$ is

$$u(\boldsymbol{\eta})\,\mathrm{d}^2\boldsymbol{\eta} = \mathrm{d}^2\boldsymbol{\eta}/4\pi. \quad (38)$$

For two points the first on a sphere surface element exposed or overlapped lying within $\mathrm{d}x$ and the second somewhere on the plane Σ_o, all values of $\boldsymbol{\rho}$ and $\boldsymbol{\eta}$ are equally likely and the probability of their falling within any specified infinitesimals of planar area $\mathrm{d}^2\boldsymbol{\rho}$ and solid angle $\mathrm{d}^2\boldsymbol{\eta}$ is

$$\frac{\mathrm{d}^2\boldsymbol{\rho}}{\Sigma_o}\,\frac{\mathrm{d}^2\boldsymbol{\eta}}{4\pi}.$$

The probability $h(x,\boldsymbol{\eta},\boldsymbol{\rho})\,\mathrm{d}^2\boldsymbol{\eta}\,\mathrm{d}^2\boldsymbol{\rho}$ also requires that the line of sight and both end points of the vector $\boldsymbol{\rho} = \mathbf{r}'-\mathbf{r}$ be free of obstruction, i.e. the probability

that no additional sphere has its center within a right circular cylinder about $\rho = \mathbf{r}' - \mathbf{r}$ capped at both ends with a hemisphere of radius q. Noting for $\rho \cdot \eta < 0$ that the point at $\mathbf{r}$ is blocked by its own sphere and using equation (34) for the probability that sphere centers are excluded from the cylindrical-hemispherical volume, we have

$$h(x,\eta,\rho)\,\mathrm{d}^2\rho\,\mathrm{d}^2\eta = \begin{cases} \{\Sigma_o/[\phi\sigma_o(x)]\}\exp[-(4\pi q^3\zeta/3)-\pi q^2\zeta\rho] \\ \qquad \times[\mathrm{d}^2\rho/\Sigma_o][\mathrm{d}^2\eta/(4\pi)] & (\text{if } \rho\cdot\eta \geqslant 0) \\ 0 & (\text{otherwise}). \end{cases} \quad (39)$$

The ratio $\phi\sigma_o/\Sigma_o$ is the probability that two points, the first on the surface, exposed or overlapped, of $\mathrm{d}x$ and the second on Σ_o, can see one another. The average entrance area $\sigma_o(x)$ that can be seen from a point on the internal surface Σ_{int} within the infinitesimal slab $\mathrm{d}x$ may be derived from the normalization of h

$$\sigma_o(x) = \pi m(m+x)\exp(-x/m). \quad (40)$$

To obtain the probability $f(x,\rho,\eta,\eta')\,\mathrm{d}^3\rho\,\mathrm{d}^2\eta\,\mathrm{d}^2\eta'$ we consider any two sphere surface points, exposed or overlapped within the slab, the first selected from the interval $\mathrm{d}x$ and the second from any other sphere with surface in the slab. Again all values of ρ, η and η' are equally likely, and the probability of falling within any specified intervals $\mathrm{d}^3\rho$, $\mathrm{d}^2\eta$ and $\mathrm{d}^2\eta'$ is

$$\frac{\mathrm{d}^3\rho}{V}\,\frac{\mathrm{d}^2\eta}{4\pi}\,\frac{\mathrm{d}^2\eta'}{4\pi}.$$

The probability that the two points are exposed and can see one another is zero unless $\rho\cdot\eta \geqslant 0$ and $\rho\cdot\eta' \leqslant 0$, since otherwise at least one point will be screened from the other by its own sphere. The probability that no other sphere has its center within a distance q of the line joining the two points, i.e. that no sphere center falls within a volume formed by a cylinder of length ρ and radius q, capped at each end by a hemisphere also of radius q, is again given by (34);

$$f(x,\rho,\eta,\eta')\,\mathrm{d}^3\rho\,\mathrm{d}^2\eta\,\mathrm{d}^2\eta' = \begin{cases} \{sV/[\phi^2\sigma_i(x)]\}\exp[-(4\pi q^3\zeta/3)-\pi q^2\zeta\rho] \\ \qquad \times[\mathrm{d}^3\rho/V][\mathrm{d}^2\eta/(4\pi)][\mathrm{d}^2\eta'/(4\pi)] \\ \qquad (\text{if } \rho\cdot\eta \geqslant 0 \text{ and } \rho\cdot\eta' \leqslant 0) \\ 0 \qquad (\text{otherwise}). \end{cases} \quad (41)$$

The ratio $\phi^2\sigma_i/(sV)$ is the probability that two exposed or overlapped surface points within the slab, the first taken within $\mathrm{d}x$ and the second from any other sphere with surface in the slab, will be exposed and able to see one another, regardless of their relative position and the orientation of their normals. Normalization of f then leads to

$$\sigma_i(x) = 8\pi m^2 - 2\pi m(2m+x)\exp(-x/m). \quad (42)$$

RESULTS AND DISCUSSION

When the probability functions (38), (39) and (41) for a random bed of overlapping solid spheres are substituted into (30) and (33) of inequality (26) and the integrals are evaluated, an upper bound on the effective bed emissivity ε_{eff} is obtained that depends on ε_s, ϕ and variational parameters μ, ω and λ. If further the parameters μ and ω are replaced by forms that minimize the upper bound, the resulting upper bound becomes the analytical function of λ, ε_s and ϕ,

$$\varepsilon_{eff} \leqslant 1 + 4(1-\varepsilon_s)\{G_1G_2G_4 - G_1^2G_5 - G_2^2G_3\} \times \{4G_3G_5 - G_4^2\}^{-1} \quad (43)$$

where

$$G_1 = -1+\phi-2\phi G_6\lambda^{-1},$$
$$G_2 = -1+\phi-4\phi G_7(3\lambda)^{-1},$$
$$G_3 = 1-\phi+2\phi\lambda^{-1}-2(1-\varepsilon_s)\phi(1-G_6)\lambda^{-1},$$
$$G_4 = 2(1-\phi),$$
$$G_5 = 1-\phi+2\phi(3\lambda)^{-1}+8(1-\varepsilon_s)\phi G_7(9\lambda^2)^{-1},$$
$$G_6 = 1-\lambda^{-1}\ln(1+\lambda),$$

and

$$G_7 = \tfrac{1}{2}-\lambda^{-1}+\lambda^{-2}\ln(1+\lambda).$$

For each surface emissivity ε_s and void fraction ϕ, a plot of the upper bound (43) vs λ gives a single minimum and associated optimum value of λ. The trial function P^* is a measure of the radiosity deviation from the internal thick bed value σT_s^4, due to the presence of a hot or cold wall. The exponential decay length (m/λ) in the trial function (27) is an approximate, average distance that wall radiation can penetrate the bed before it is absorbed. Optimum values of λ are given vs the void fraction for various values of the surface emissivity in Fig. 2(a). That λ is roughly 2 for a nearly black surface ($\varepsilon_s \sim 1.0$) is consistent with absorption on first surface collision. As the emissivity decreases from unity, the λ optimum decreases because increased surface reflection allows a deeper penetration into the bed. A very mild variation of λ with the void fraction (7.7% for $\phi = 0.99$) nearly disappears for surface emissivities below 0.1.

The optimum variational effective bed emissivity ε_{eff} is shown in Fig. 2(b) vs the void fraction ϕ for various surface emissivities ε_s. As the void fraction goes to zero the overlapping sphere bed becomes a solid block and the bed emissivity ε_{eff} is equal to the surface emissivity ε_s. Of particular interest in Fig. 2(b) is the nearly linear relationship between the bed emissivity variational result and the void fraction, Borodulya and Kovensky [9] have already suggested that the fluidized bed emissivities should depend on the void fraction. For any ε_s on Fig. 2(b), a straight line can be drawn through the emissivity curve end points at $\phi = 0$ and 1.0. A measure of its deviation from the variational value at any ε_s and ϕ, the variational emissivity minus

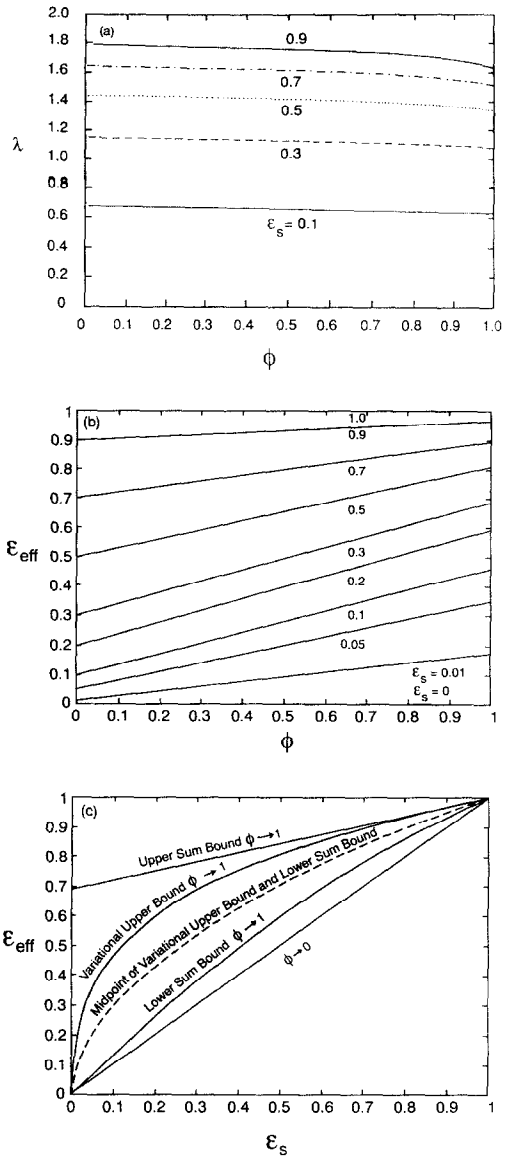

FIG. 2. (a) Optimum values of the parameter λ vs the void fraction ϕ at various particle surface emissivities ε_s; (b) effective bed emissivity ε_{eff} vs the void fraction ϕ for various particle surface emissivities ε_s; (c) the upper sum bound (44), lower sum bound (45), variational upper bound (43), and midpoint estimate of the effective emissivity ε_{eff}, all at unit void fraction ($\phi \to 1$), vs the solid surface emissivity ε_s. The midpoint estimate is given as a dashed line and the error bounds are shaded. Also the straight diagonal line is the exact bed emissivity at $\phi = 0$.

the straight line value divided by the linear result, is usually quite small with a maximum absolute value of only 2.1×10^{-4} located at $\varepsilon_s = 0.3$ and $\phi = 0.52$. In the two limits of perfect absorption $\varepsilon_s \to 1$ and complete reflection $\varepsilon_s \to 0$, the effective emissivity of a semi-infinite random bed or porous slab does not depend on the void fraction, and the exact effective emissivity values lie, respectively, on the top and bottom horizontal edges of Fig. 2(b). For ε_s values between these limits, increasing the bed void fraction always enhances the effective emissivity. The variational bed emissivity ε_{eff} exhibits a mildly positive slope in the void fraction, that monotonically increases from zero at $\varepsilon_s = 0$, goes through a maximum value of 0.395 at $\varepsilon_s = 0.21$, and then monotonically decreases back to zero at $\varepsilon_s = 1.0$.

Figure 2(c) examines the relationship of the variational ε_{eff} with the particle surface emissivity ε_s for fixed void fractions. From Fig. 2(b) for any ε_s, the variational upper bound value of ε_{eff} is a maximum in the dilute bed limit ($\phi \to 1$), and in Fig. 2(c) a curve of these maxima is drawn. Included for comparison in Fig. 2(c) are complementary upper and lower bounds on ε_{eff} for same random void–solid geometry, derived in ref. [16] from truncated summation representations of ε_{eff},

$$\varepsilon_{eff} \leqslant \varepsilon_s + 0.6902(1-\varepsilon_s)\phi \tag{44}$$

and

$$\varepsilon_{eff} \geqslant \varepsilon_s + 0.3804\varepsilon_s(1-\varepsilon_s)\phi. \tag{45}$$

As with the variational result, both (44) and (45) have a positive void fraction slope which depends only on ε_s, and their largest values, which occur at $\phi \to 1$, are given in Fig. 2(c). All three expressions (43)–(45) for ε_{eff} decrease linearly with ϕ to the diagonal line at $\phi = 0$ in Fig. 2(c). At this level of computation, the variational upper bound principle is a clear improvement over the upper sum bound for any ε_s or ϕ. However, with improvement the upper sum will give the best bounds in the neighborhood of unit surface emissivity where the sum is exact. Note also that a better upper sum bound is automatically generated when an improved lower sum bound is calculated [16]. The variational principle upper and lower sum bounds provide a squeeze on the possible values of ε_{eff}. A midpoint estimate dashed line and as well as shaded error bounds are also included in Fig. 2(c) for the case $\phi \to 1$. Note that the maximum error is shown in Fig. 2(c), as all four curves drop linearly with ϕ to the diagonal $\phi = 0$ line, the error region shown for $\phi \to 1$ decreases by a factor ϕ at any lower void fraction. To obtain ε_{eff} estimates at intermediate ϕ from Fig. 2(c), the vertical distance, measured from the diagonal to the curve at a fixed ε_s and multiplied by ϕ, must be added to the diagonal value ε_s.

Figure 3(a) compares the variational upper (43) and lower sum bounds (45) on ε_{eff}, calculated for a semi-infinite slab cut from a bed of randomly placed, freely overlapping spheres all of the same radius, to effective emissivity curves for packed and expanded cubic lattices of spheres calculated by the cell model approximation [8, 9], and to bed emissivities obtained from the two-flux model [5, 6]. At intermediate void fractions, $\phi \sim 0.2$–0.6, the overlapping sphere bed resembles the edge of a pellet of compressed smaller particles. For a void fraction of 0.4 in Fig. 3(a), the solid variational upper bound and dashed lower truncated sum bound lie close enough that a mid-curve estimate gives a reasonably good picture of the

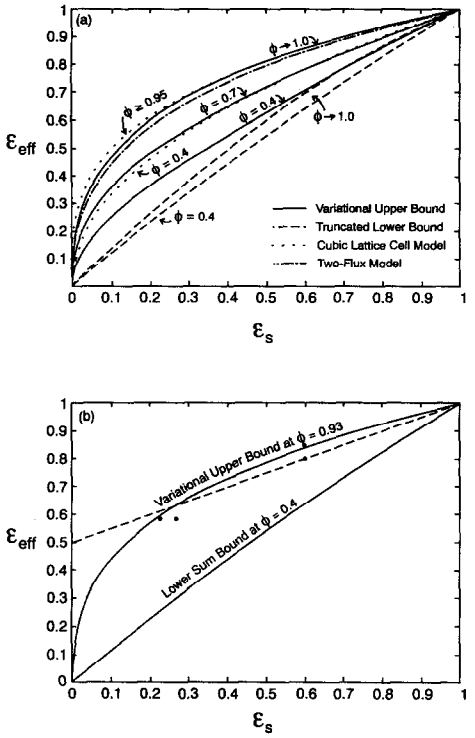

FIG. 3. (a) Comparison of overlapping sphere effective emissivity calculations with cell model and two-flux model calculations. Solid curves are variational upper bounds (43) for ε_{eff} vs ε_s at void fraction $\phi \to 1$, $\phi = 0.7$ and $\phi = 0.4$. The dashed line curves are truncated sum lower bounds (45) at $\phi \to 1$ and $\phi = 0.4$. The dotted curves are all cell model calculations [8, 9] done for a cubic lattice of spheres at $\phi \geq 0.95$ and $\phi = 0.4$. The dashed–dot curve is from the two-flux model [5, 6]; (b) Comparison of the overlapping sphere effective emissivity bounds with a suggested correlation and experimental data. Solid curves are the variational upper bound (43) for $\phi = 0.93$ and lower sum bound (45) for $\phi = 0.4$. The dashed line is a correlation by Grace [13] and the data points are from Botterill [3].

ε_{eff} curve. The packed cubic lattice, cell model dotted curve has the same shape as the estimate from the bounds, but lies well above the random sphere bounds. The ordered structure of the cubic lattice gives a larger ε_{eff} due to the open channels that allow deeper radiation penetration. In general, ε_{eff} values at intermediate void fractions will be sensitive to surface structure. At high void fraction ($\phi \to 1$) sphere overlap becomes unlikely, the Σ_{ext} term in both Ψ and Λ vanish due to the $(1-\phi)$ factors in (29) and (33), and the randomly overlapping sphere model relates exactly to a gray gas [10, 16] or an idealized dilute fluidized bed of randomly placed solid spheres. Both the expanded cubic lattice ($\phi \geq 0.95$) cell model dotted curve and the dot–dash two-flux bed emissivity curves lie well above the rigorous variational upper bound for $\phi = 0.4$ and 0.7 and are grouped around the variational solid curve for $\phi \to 1$. Hence, as expected, both of these approximate model emissivity curves apply only to dilute beds. The two-flux curve in Fig. 3(a) lies rather close to the variational result for $\phi = 0.95$. At $\varepsilon_s = 0.01$ the two-flux model curve lies 4.1% below the variational curve for $\phi = 0.95$, approaches and crosses over it at $\varepsilon_s = 0.62$. The upper part of the two-flux curve lies always above, but very close to the variational curve for $\phi = 0.95$ (differing by at most 0.07%). Due to the open channels the lattice curve is slightly above both of the corresponding random model results.

We have selected for simplicity a thick slab cut from a very large bed of randomly placed, freely overlapping spheres as a model solid dispersion to illustrate the effective bed emissivity variational principle and summation lower bound. While this a somewhat idealized case to compare with a fluidized bed, the calculations do treat multiple reflections within a random particulate media in a rigorous manner and represent a gray gas for high void fractions, so it is of some interest in Fig. 3(b) to compare the emissivity bounds (43) and (45) to a correlation and several experimental bed emissivities [3] for fluidized beds. While corresponding particle emissivities are listed, no void fraction information is available for either the correlation or the data. Borodulya and Kovensky [9] have suggested a bed porosity range from 0.4 to 0.93 as appropriate for a fluidized bed. The variational upper bound for 0.93 and the lower sum bound for 0.4 are drawn in Fig. 3(b), respectively, as the extreme upper and lower solid curves to bound any experimental results. The dashed straight line is a well-known linear correlation suggested by Grace [13] and the four data points are from Botterill [3]. The data points were given in the literature without tabulated void fractions, and as the points lie very close to or within the voidage range, agreement is satisfactory. Indeed if we select the $\phi \to 1$ variational upper bound, all data points lie within the bounds, and we can reasonably speculate that the data was from rather dilute fluidized beds.

SUMMARY AND CONCLUSIONS

A rigorous theory of wall to bed radiative heat transfer has been formulated for a semi-infinite, isothermal void–solid bed. A variational principle has been derived, that gives an upper bound in the effective bed emissivity. The variational integrals are written in terms of the fundamental statistical properties of the random solid needed to estimate the effective bed emissivity. Explicit results are presented for a semi-infinite slab cut from a bed of randomly placed, freely overlapping solid spheres, all of the same radius. The variational effective emissivity was shown to increase linearly with the void fraction, and the slope was dependent on the particle surface emissivity. The variational upper bound effective emissivity results were compared with upper and lower bound truncated summation bounds recently obtained for the same model structure [16]. While the variational principle gives a better upper bound, for improved calculations the upper sum will give a better bound near the black

surface limit where both sums are exact. The variational upper bound and the lower sum bound provide a rigorous squeeze on the effective emissivity curves, which tightens with decreasing void fraction. These reciprocal bounds when compared with cell model and two-flux bed emissivities gave qualitative insight for any void fraction, but in dilute random sphere beds the agreement was quantitative. Results also compared favorably with an empirical equation and measured experimental bed emissivities.

REFERENCES

1. A. Varma, G. Cao and M. Morbidelli, Self-propagating solid–solid non-catalytic reactions in finite pellets, *A.I.Ch.E. Jl* **36,** 1032–1038 (1990).
2. J. Szekely and J. W. Evans, A structural model for gas–solid reactions with a moving boundary—II. The effect of grain size, porosity and temperature on the reaction of porous pellets, *Chem. Engng Sci.* **26,** 1901–1913 (1971).
3. J. S. M. Botterill, *Fluid-Bed Heat Transfer*. Academic Press, New York (1975).
4. G. Flamant, Theoretical and experimental study of radiant heat transfer in a solar fluidized-bed receiver, *A.I.Ch.E. Jl* **28,** 529–535 (1989).
5. M. Q. Brewster, Effective emissivity of a fluidized bed, HTD-40, *ASME Winter Annual Meeting*, New Orleans, Louisiana, pp. 7–13 (1984).
6. M. Q. Brewster, Effective absorptivity and emissivity of particulate media with application to a fluidized bed, *ASME J. Heat Transfer* **108,** 710–713 (1986).
7. C. L. Tien and B. L. Drolen, Thermal radiation in particulate media with dependent and independent scattering. In *Annual Review of Numerical Fluid Mechanics and Heat Transfer*, Vol. 1, pp. 1–32. Hemisphere, New York (1986).
8. V. A. Borodulya, V. I. Kovensky and K. E. Makhorm, Fluidized bed radiative heat transfer, *Proceedings of 4th International Conference on Fluidization* (Edited by D. Kunii and R. Toei), pp. 379–387. Engineering Foundation, New York (1983).
9. V. A. Borodulya and V. I. Kovensky, Radiative heat transfer between a fluidized bed and a surface, *Int. J. Heat Mass Transfer* **26,** 277–287 (1983).
10. R. Siegel and J. R. Howell, *Thermal Radiation Heat Transfer*. McGraw-Hill, New York (1992).
11. D. Vortmeyer, Radiation in packed solids, *German Chem. Engng* **3,** 124–138 (1980).
12. S. C. Saxena, K. K. Srivastava and R. Vadivel, Experimental techniques for the measurement of radiative and total heat transfer in gas fluidized beds: a review, *Experimental Thermal and Fluid Sci.* **2,** 350–364 (1989).
13. J. R. Grace, Fluidized bed heat transfer. In *Handbook of Multiphase Systems* (Edited by G. Hestroni), pp. 8–72. Hemisphere, New York (1982).
14. W. Strieder and R. Aris, *Variational Methods Applied to Problems of Diffusion and Reaction*. Springer, Berlin (1973).
15. S. Torquato, Random heterogeneous media: microstructure and improved bounds on effective properties, *Appl. Mech. Rev.* **44,** 37–76 (1991).
16. Y. Xia and W. Strieder, Complementary upper and lower bounds on the effective emissivity *Int. J. Heat Mass Transfer* **37,** 443–450 (1994).
17. J. J. Carberry, *Chemical and Catalytic Reaction Engineering*. McGraw-Hill, New York (1976).
18. N. Decker and L. R. Glicksman, Conduction heat transfer at the surface of bodies immersed in gas fluidized beds of spherical particles, *A.I.Ch.E. Symp. Series*, Vol. 77, No. 208, pp. 341–349 (1981).
19. N. Decker and L. R. Glicksman, Heat transfer in large particle fluidized beds, *Int. J. Heat Mass Transfer* **26,** 1307–1320 (1983).